Laser desorption mass spectrometry with an Orbitrap analyser for in situ astrobiology

Ricardo Arevalo, Lori Willhite, Anaïs Bardyn, Ziqin Ni, Soumya Ray, Adrian Southard, Ryan Danell, Andrej Grubisic, Cynthia Gundersen, Niko Minasola, et al.

Laser Desorption Mass Spectrometry with an Orbitrap Analyzer for *in situ* Astrobiology

Ricardo Arevalo Jr.[1,2], Lori Willhite[2], Anais Bardyn[2], Ziqin Ni[2], Soumya Ray[2], Adrian Southard[3], Ryan Danell[4], Andrej Grubisic[5], Cynthia Gundersen[6], Niko Minasola[6], Anthony Yu[5], Molly Fahey[5], Emanuel Hernandez[5], Christelle Briois[7], Laurent Thirkell[7], Fabrice Colin[7], and Alexander Makarov[8]

[1]Corresponding Author: rarevalo@umd.edu

[2]University of Maryland, College Park, MD USA

[3]CRESST II, College Park, MD USA

[4]Danell Consulting, Winterville, NC USA

[5]NASA Goddard Space Flight Center, Greenbelt, MD USA

[6]AMU Engineering, Miami, FL USA

[7]Laboratoire de Physique et Chimie de l'Environnement et de l'Espace, Orléans, FR

[8]Thermo Fisher Scientific, Bremen, DE

Title: 85 characters (w/ spaces)

Abstract*:* 150 words

Main text: 3246 words

Display items: 5 figures

References: 52 total (50 in main text)

Keywords: astrobiology; biomarker; life detection; mass spectrometry; Enceladus; Europa; ocean worlds

Abstract (limit 150 words unreferenced; currently 150 words)

Laser desorption mass spectrometry (LDMS) enables *in situ* characterization of the organic content and chemical composition of planetary materials without requiring extensive sample processing. Coupled with an Orbitrap™ analyzer capable of ultrahigh mass resolving powers and accuracies, LDMS techniques facilitate the orthogonal detection of a wide range of prospective biomarkers and classification of host mineralogy. Here, an Orbitrap LDMS instrument that has been miniaturized for planetary exploration is shown to meet the performance standards of commercial systems and exceed key figures of merit of heritage spaceflight technologies, including those baselined for near-term mission opportunities. Biogenic compounds at area densities relevant to prospective missions to ocean worlds are identified unambiguously by redundant measurements of molecular ions (with and without salt adducts) and diagnostic fragments. The derivation of collision cross-sections serves to corroborate assignments and inform on molecular structure. Access to trace elements down to ppmw levels provide insights into geological context.

Main text (upper limit 3500 words, excl. abstract, methods, references and legends)

Future astrobiology missions to Europa, Enceladus, and other potentially viable ocean worlds will be challenged to distinguish biological signatures without bias towards features associated with terrestrial life [1]. Payload instruments need to support agnostic and discovery-based approaches to distinguish relics of biological processes from the limited complexity and apparent randomness of abiotic sources [2]. A critical capability of next-generation technologies will be the orthogonal (or independent) detection of a variety of biomarkers, including (but not limited to): organic abundance patterns; stable isotope ratios; biogenic minerals; and, morphologies indicative of microbial activity [3]. Multiple distinct proxies observed across a range of spatial scales provide a framework to gauge the probability of biogenicity [4].

Laser desorption mass spectrometry (LDMS) enables investigations into the organic inventory and the elemental/isotopic composition of planetary materials *in situ*, providing: i) access to multiple classes of biomarkers, most notably refractory organic matter; and, ii) identification of host mineralogy, ergo geological context for detected organic compounds. Unsupervised data-driven approaches can increase operational autonomy and enhance the confidence in organic/inorganic assignments (e.g., [5]). Laser microprocessing is well suited for life detection objectives as such methods require minimal sample processing and support 2D chemical imaging without requiring physical contact with the sample; standoff instruments reduce the risk of cross-contamination and planetary protection violations. The spatial resolution of an LDMS experiment is controlled by the profile of the beam focused onto the sample surface, allowing for targeted analyses of micron-scale mineral phases, individual dust particles, microfossils, finely laminated biofabrics, and discrete strata captured in sample cores. Each laser shot only ablates the uppermost <100 nm of the sample even at elevated fluences (e.g., [6]), resulting in an effective sample mass on the order of ng; thus, LDMS is ideal for surface analysis and/or depth profiling. However, this can be a limiting capability if bulk measurements are required to meet specific planetary science objectives.

Due to these analytical advantages, a standoff LDMS instrument called LIMA-D was launched onboard Phobos 2 in 1988; however, communication with the spacecraft was lost during the approach towards Phobos, compromising the mission [7]. A derivative of LIMA-D, named LAZMA [8], was later launched in 2011 onboard the Phobos-Grunt mission, but a propulsion failure left the spacecraft stranded in low Earth orbit. Thus, LDMS techniques have yet to be applied in an extraterrestrial planetary environment. However, LDMS instruments have been developed for the ExoMars rover [9], Dragonfly rotorcraft [10], and Luna-Glob (Luna-25) and Luna-Resurs-1 (Luna-27) missions [11], illustrating the impetus to exploit such *in situ* techniques to address high-priority science questions in the planetary community.

Here, we describe an LDMS instrument that combines an Orbitrap™ mass analyzer, solid-state UV (266 nm) laser system derived from heritage designs, and custom series of ion optics that accelerate and focus ions generated at the sample surface into the analyzer. A prototype of the LDMS instrument (**Fig. 1**) has been highly miniaturized relative to the proof-of-concept breadboard reported previously [12] but without a compromise in analytical performance (as discussed further below), representing an engineering model of a spaceflight design that fits within the limited resources expected for a mission to the outer Solar System (*e.g.*, the Europa Lander [13]; see Supplement).

The Orbitrap analyzer, originally developed for commercial laboratories [14] but recently adapted for planetary applications [12], delivers 100× higher mass resolution and mass accuracy compared to the legacy quadrupole sensors that have explored the inner and outer reaches of the Solar System [15]. Such analytical capabilities are essential to separate isobaric interferences (defined by the same nominal mass-to-charge ratio, or integer *m/z*) and unambiguously identify molecular stoichiometry without additional

subsystems (*e.g.*, resonance lasers and gas chromatographs). Because the Orbitrap analyzer uses electrostatic fields to trap ions [16], the sensor does not require magnets, RF electronics, or consumable detectors, limiting failure modes and minimizing resource requirements. The basic operation of the Orbitrap analyzer involves injection and trapping of analyte ions, which then exhibit harmonic axial oscillations at frequencies proportional to $(m/z)^{-½}$. Ion motion recorded as image current in the time domain transient can be converted into frequency space via fast Fourier transform (FFT).

The effective mass range in a given experiment is influenced by the distance the ions travel from the source to the trap, and the timing and slew rate of the voltages applied to the center and deflector electrodes, which together enable electrodynamic squeezing of the incoming ions [14]. During an LDMS analysis, the primary limit to the upper end of the mass range is the capacity of the laser source to ionize macromolecular organic material without incurring excessive fragmentation of the parent molecule. The mass resolving power is controlled principally by the observation time (*i.e.*, transient length) and temporal spread within a single *m/z* ion packet. Given these timing requirements and sensitivity to temporal smearing, a pulsed laser system is a natural choice to serve as an ion source.

Previously, an Orbitrap analyzer extracted from its commercial packaging and interfaced directly to an industrial laser was shown to characterize the mineralogy of a variety of planetary analog samples and detect amino acids down to < 100 fmol/mm^2 concentrations (based on signal-to-noise ratios) with only a single laser shot and no spectral stacking [17]. However, this breadboard was not designed to minimize mass, volume, and power requirements, but rather to validate experimentally the scientific reach of LDMS techniques that leverage an ultrahigh resolution mass analyzer.

In comparison, the footprint of the LDMS instrument described here has been miniaturized for mission science by interfacing an Orbitrap analyzer with a laser system that leverages the side-pumped Cr:Nd:YAG oscillator design flown on the Lunar Orbiter Laser Altimeter (LOLA) [18], with a fundamental wavelength of 1064 nm and nominal pulse width of 5 ns. A fourth harmonic generator produces an output wavelength of 266 nm (4.7 eV/photon), enhancing photon-substrate coupling with aromatic organics [19] and many geological phases [20]. The laser generates >450 μJ/pulse at 266 nm [21], more than three times the maximum energy of the laser for the state-of-the-art Mars Organic Molecule Analyzer (MOMA) instrument onboard the ExoMars rover [9]. Fine attenuation control down to 1% of the maximum output energy is achieved by controlling the polarization of incident 532 nm light prior to conversion to 266 nm in the fourth harmonic; for comparison, the MOMA laser output energy can only be reduced to 10% of the maximum value by thermal detuning of the fourth harmonic crystal [22].

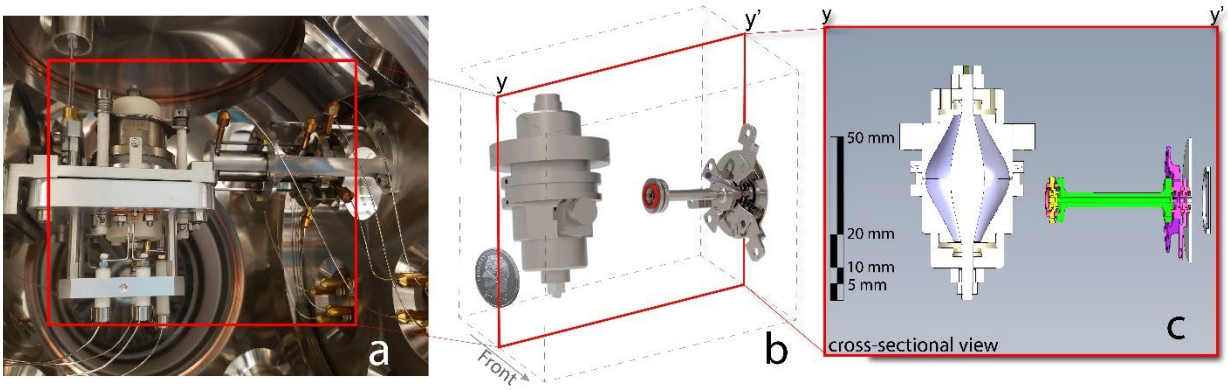

Fig. 1. A prototype of the highly miniaturized Orbitrap LDMS instrument described here, which has been designed to minimize mass, volume, and power requirements without compromising the capabilities of the proof-of-concept breadboard reported previously [12], exceeds key performance metrics of the MOMA flight instrument [9], including: mass resolution and accuracy; laser output energy; and dual polarity ion detection. (a) Photograph of the Orbitrap analyzer and ion optical lenses mounted within a planetary simulation chamber. (b) Solid model and (c) cross-sectional view showing the orientation and compact geometry of the analyzer, lens stack, and sample plate.

A longstanding issue for LDMS techniques has been the deduction of quantitative information, particularly relative and absolute abundances of elemental and molecular species. The reproducibility of LDMS peak intensities is limited by: i) the heterogeneity of the sample; ii) shot-to-shot variability of the laser output energy; and, iii) dynamic changes in sample morphology induced by extended laser irradiation, which affect photon-substrate coupling. However, the empirical determination of *relative sensitivity factors* of elements with distinct electronic configurations, which have been shown to control laser induced fractionation [23], can enable the quantification of concentration ratios (*e.g.*, [24]) in solid samples. Absolute abundances can be further derived if an internal standard is known (*e.g.*, [25]). Such approaches, which are commonplace for laser ablation inductively coupled plasma mass spectrometry (LA-ICPMS), offer promise for the quantitation of spectral signals derived from LDMS analysis. However, significant work remains to validate these models.

Measuring the relative abundances of organic molecules is even more challenging as observed signal intensities are sensitive to the absorption characteristics, bond strengths, and ionization energy of the compound, as well as the physicochemical properties of the sample matrix and dynamics of the plasma plume. In spite of these challenges, linear responses between analyte concentrations and peak intensities normalized to an internal standard have enabled the quantitative analysis of amino acids [26], oligonucleotides [27], and a range of other organics (*e.g.*, [28]) via LDMS techniques.

Due to their identical electronic configurations and comparable physicochemical properties, isotopes of the same element (and isotopologues of the same molecule, to a lesser extent) are more easily preserved during an LDMS experiment. Isotopic precision is controlled largely by signal-to-noise ratios, and thus the dynamic range of the sensor. The Orbitrap analyzer, which can accommodate up to 10^6 elementary charges during a single analysis [29], has been shown to support a linear intrascan dynamic range up to 10^4 [30], providing access to low abundance isotopes down to 0.1 mol%. Although space charge effects can incur isotope fractionation during transient acquisition (*e.g.*, [31]), precise and accurate $^{13}C/^{12}C$ ratios measured for single species (e.g., $^{13}C^{12}C_2H_8O_2N^+/^{12}C_3H_8O_2N^+$ in nominally pure alanine) within

multicomponent sample mixtures have been recorded following careful calibration efforts, such as mass pre-filtering, transient length shortening, and/or external standardization with a matrix-matched reference material [32].

Results

A typical LDMS experiment comprises: i) desorption/ionization of the sample via pulsed laser light; ii) acceleration, focusing, and adjustment of the reference potential of analyte ions through the ion optics lens stack; iii) ion injection and electrodynamic squeezing in the trap; and, iv) detection of ion packets according to their respective axial frequencies, and hence *m/z*. Tunable laser energy (and by extension fluence, J/cm^2, and irradiance, W/cm^2) promotes the ionization of refractory organics and mineral phases via multiphoton absorption, supporting controlled fragmentation and disproportionation reactions to derive molecular structure by in-source decay (e.g., [33]). The beam radius at the sample surface (r) is a customizable parameter within the limits of diffraction; with an effective focal length of 140 mm, nominal UV beam diameter of 3.0 mm, and beam quality factor $M^2 < 1.5$, the 266 nm laser system leveraged in this study could approach a diffraction limited radius of $r < 12$ µm. Such fine spatial resolution comes at the expense of total analyte throughput, which tracks with r^2 at a given fluence/irradiance. A MEMS steering mirror inside the laser head, coupled with a set of deflector electrodes within the ion optics, allows the construction of 2D chemical images with a nominal 500 µm diameter field of view (see Supplement) without requiring translation/rotation of the sample, facilitating the identification of biofabrics *in situ*.

The measurement of both positively and negatively charged particles provides complementary perspectives of complex chemical mixtures, empowering the detection of organic molecules with acidic and basic side chains, as well as mineralogical indicators with high and low electronegativities. For example, positive and negative mass spectra of a finely ground CsI disc (**Fig. 2**), a common laboratory standard with identical composition to the calibrant for the MOMA flight instrument, provide multiple molecular fingerprints diagnostic of the substrate. In positive mode, CsI is exemplified by a high intensity Cs^+ peak (*m/z* 132.9054), but also $Cs(CsI)^+$ (*m/z* 392.7153) and $Cs(CsI)^{2+}$ (*m/z* 652.5253) clusters at lower signal intensities. In negative mode, the spectrum is dominated by I^- (*m/z* 126.9045) followed by $I(CsI)^-$ (*m/z* 386.7144) and $I(CsI)^{2-}$ (*m/z* 646.5243). The mass resolution (*e.g., m/Δm* >100,000, FWHM at Cs^+) and ppm-level mass accuracy of these spectra, collected on the miniaturized prototype shown in **Fig. 1**, meet the performance specifications of commercial instruments; for example, the Thermo Q Exactive™ offers mass resolution up to *m/Δm* = 140,000 (FWHM) at *m/z* 200 with < 3 ppm mass accuracy (RMS with external calibration). Such analytical capabilities support the unambiguous identification of elemental and molecular signatures for both commercial and spaceflight applications.

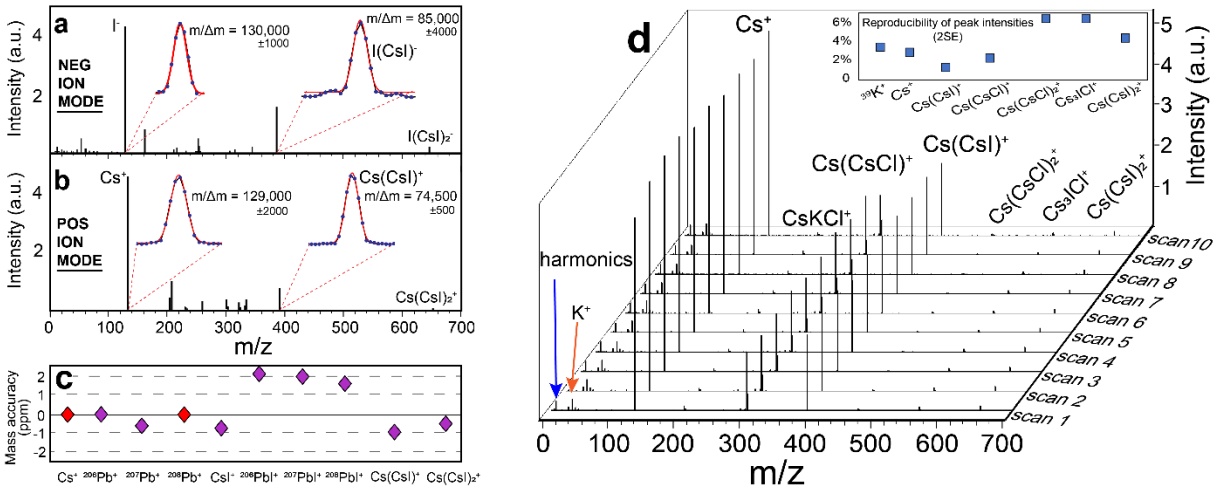

Fig. 2. In both negative and positive mode, the miniaturized Orbitrap LDMS instrument achieves mass resolving powers ($m/\Delta m$ > 10^5, FWHM at m/z 100) comparable to commercial standards. (a, b) Spectra represent averages of 10 scans in the time domain, each acquired with an 800 ms transient (high-resolution) and sampling rate of 5 MHz (see Methods). Reported uncertainties of the mass resolving powers of individual peaks are determined by the fit of a Gaussian curve to the raw data. (c) Using $^{133}Cs^+$ as a single point internal standard, and subsequently $^{133}Cs^+$ and $^{208}Pb^+$ to apply a secondary linear calibration, peaks fall within ppm of exact monoisotopic masses. (d) Ten single scans collected in positive mode, acquired sequentially with 200 ms transients (medium-resolution) and 5 MHz sampling rate, illustrate the reproducibility of the experiments (see Supplement). As shown in the inset, the peak intensities of $^{39}K^+$, Cs^+, and $Cs(CsI)^+$ all vary by less than 5% (2SE) across all scans. Irradiance 0.1 GW/cm^2.

Chloride salts, such as NaCl and KCl, are important planetary materials because they can depress the freezing point of liquid water in cryogenic environments and concentrate dilute monomers of more complex biomolecules (*e.g.*, RNA) via enhanced adsorption onto mineral surfaces [34]. Such salts have been observed on the surface of Europa [35], within the Enceladus plume [36], and inside Occator crater on the dwarf planet Ceres [37]. Consequently, to address high-priority astrobiology mission objectives [38, 39], future payload investigations need to characterize salt-rich sample matrices to gain insights into the provenance of detected organics.

Assuming the composition of Enceladus approximates that of a comet, as suggested by comparable volatile abundances and D/H ratios recorded in the plume [40] and those observed in cometary comae [41], measurements provided by the Cassini payload implicate up to ppmw concentrations of individual amino acids in the subsurface ocean [42]. Area densities exceeding 200 pmol/mm^2 are projected if 1 mL of water ice, the sample volume baselined for each instrument onboard the Europa Lander [38], was sublimated onto a cm^2 sample plate. The analysis of a salt-rich planetary analog sample containing similar levels of a proteinogenic amino acid (*i.e.*, histidine) and nucleobase (*i.e.*, thymine) demonstrates the capacity of the Orbitrap LDMS instrument to simultaneously access both organic and inorganic fractions of multicomponent sample mixtures representative of those that may be collected by future missions to ocean worlds (**Fig. 3**).

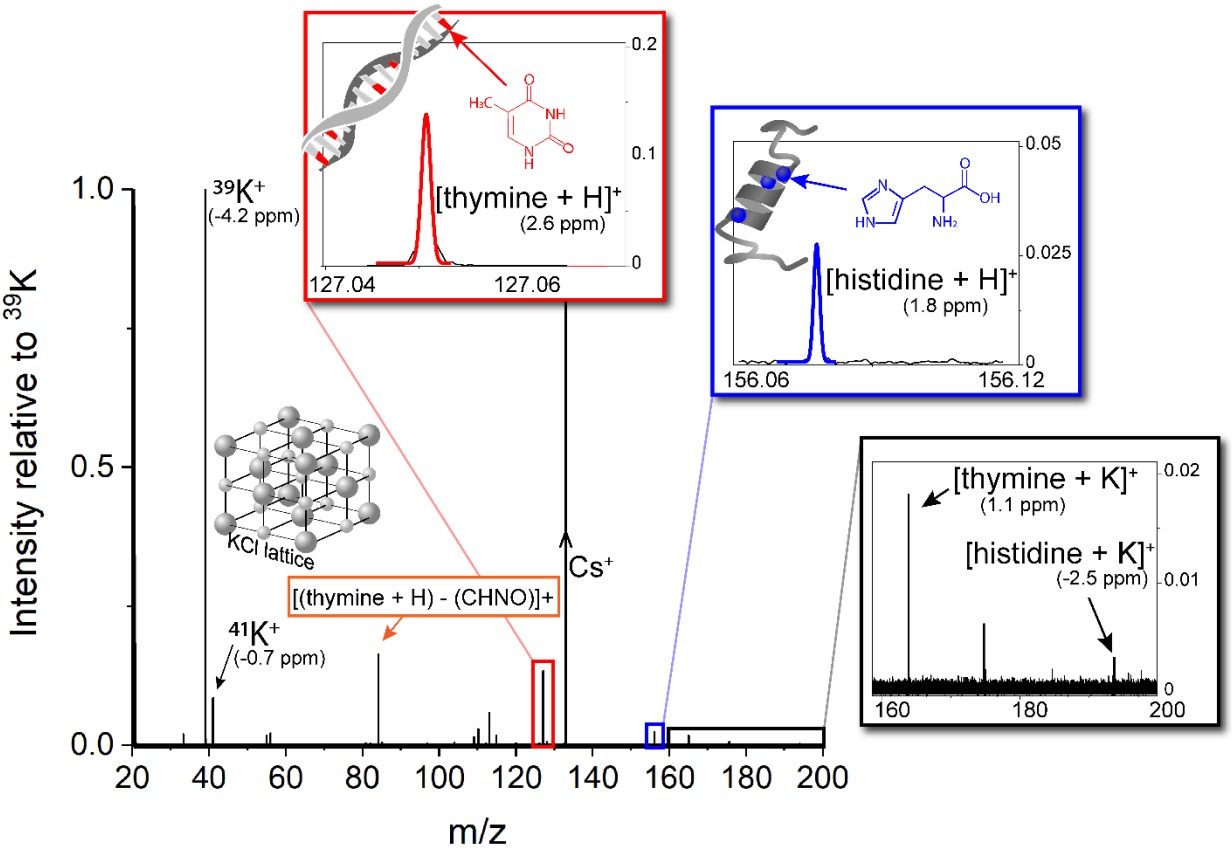

Fig. 3. Analysis of a residue of a salt-rich (0.32 wt.% KCl) solution doped with trace levels of thymine and histidine, both prospective biomarkers containing aromatic groups that effectively absorb UV radiation (see Supplement), without desalination of the sample. The area densities of thymine (180 pmol/mm^2) and histidine (210 pmol/mm^2) approximate those expected if 1 mL of ice derived from Enceladus' subsurface ocean was sublimated onto a cm^2 sample plate (see main text). Detection of protonated molecular ions ([M+H]$^+$ shown with Gaussian fits), diagnostic fragments ([M+H-CHNO]$^+$), and potassiated peaks (*e.g.*, [M+K]$^+$) provide corroborative identification of the analytes. The isotopic composition of K derived from the salt matrix falls within natural values. This spectrum represents a single scan acquired with an 800 ms transient and sampling rate of 5 MHz. ^{133}Cs$^+$, sourced from the collocated CsI target, was used as an internal standard; ^{39}K$^+$, ^{133}Cs$^+$, and ^{208}Pb$^+$ were used to apply a linear calibration. Irradiance 0.3 GW/cm^2.

The elucidation of molecular structure, including the differentiation of structural isomers, represents an orthogonal means to establish the identity of prospective biomarkers and inform on the probability of biogenicity based on molecular complexity [2]. The finely controlled output of the laser source pioneered here enables in-source decay, a technique that has been shown to induce molecular fragmentation and facilitate the identification of peptides based on diagnostic amine-bond cleavages [43], and sequencing of proteins from the determination of N-terminal fragments [44] via matrix-assisted LDMS techniques. Another emerging capability specific to the Orbitrap analyzer involves determining the distinct decay rate of each compound during time-resolved transient signal acquisition in order to calculate of collision cross

section (CCS), a measure of ion size and conformation unique to each chemical species [45]. As a packet of ions of a specific *m/z* oscillates around the center electrode, individual ions de-phase due primarily to elastic collisions with background gas, ion-ion interactions, and other factors (*e.g.*, high-voltage ripple and field perturbations derived from mechanical imperfections) [46]. The additive effect of these processes results in degradative signal loss of ion packets as a function of time within the analyzer.

As shown in **Fig. 4**, the decay profiles of select chemical species identified in **Fig. 3** can be extracted from a single transient spectrum via FFT, followed by inverse FFT. The observed signal losses reflect the specific experimental conditions (*e.g.*, pressure, temperature, and voltages) in addition to the additive decay factors described above. Chemical species that exhibit faster decay rates represent compounds with larger cross-sections, which reflect both *m/z* and molecular structure. Previous work has shown that the cross-sections of biogenic amino acids directly correlate with molecular weight, but aliphatic and aromatic compounds tend to be larger than the average trend due to inefficient folding [47]. Thus, CCS determinations provide a complementary means to identify organic compounds and differentiate molecular structures, supporting agnostic detection techniques for the characterization of putative biomarkers.

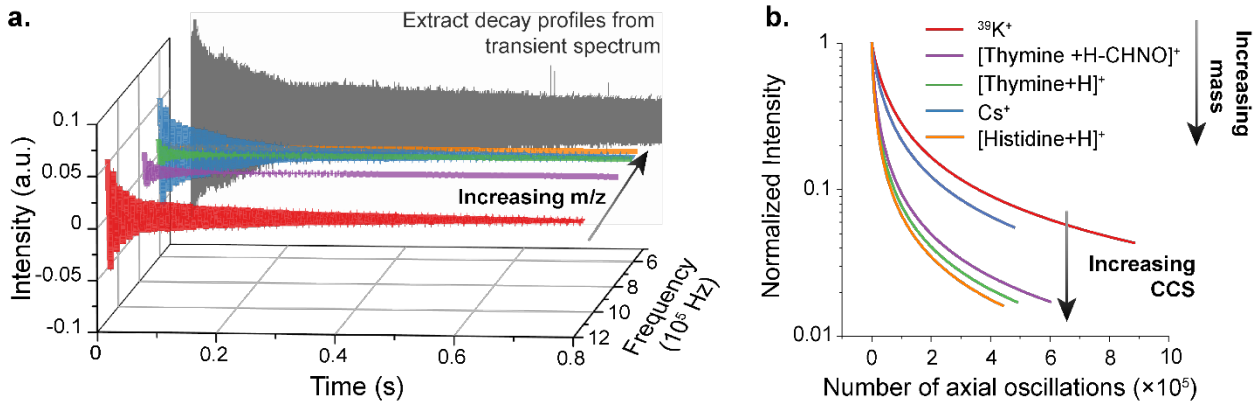

Fig. 4 (a) The total transient signal (grey) may be decomposed into decay profiles of individual chemical species based on their distinctive frequencies (or *m/z*) via FFT and subsequent inverse FFT. The signal intensities of select peaks identified in Fig. 3 correlate with ion abundances (and to a lesser extent radial distribution about the center electrode). (b) The decay rates of signal intensities reflect ion losses as a function of time, informing on molecular weight and structure.

The detection of organic compounds alone is insufficient to characterize the habitability potential of a cryogenic environment and/or assign prospects for extant or extinct life with high confidence. Exogenous infall can deliver significant quantities of organic material to the surface of any planetary body; for reference, more than 10^7 kg of exogenous material is delivered to the Earth every year [48]. Although infall rates scale with planet mass and interplanetary dust fluxes vary as a function of heliocentric distance [49], significant quantities of organic materials are continually being accumulated on Europa, Enceladus, and other ocean worlds. Associations between detected organic compounds and host mineralogy, informed by major, minor and trace element abundances, are powerful tools for establishing the provenance of organic matter. Rare earth elements (REE; *i.e.*, La through Lu) are particularly valuable proxies for geological sources as this suite of trace elements shares a common valence state (X^{3+}) and systematic contraction in ionic radii, resulting in predictable partitioning behaviors. Consequently, REE

are routinely used to understand the chemistry, formation, and evolution of major terrestrial reservoirs [50]. The miniaturized LDMS described here can measure REE down to ppmw levels in solid samples (**Fig. 5**), enabling insights into the sourcing of detected organic molecules, including prospective biomarkers. However, a systematic evaluation is needed to constrain the accuracy of quantified elemental concentrations and the reproducibility of observed abundance patterns of organic molecules.

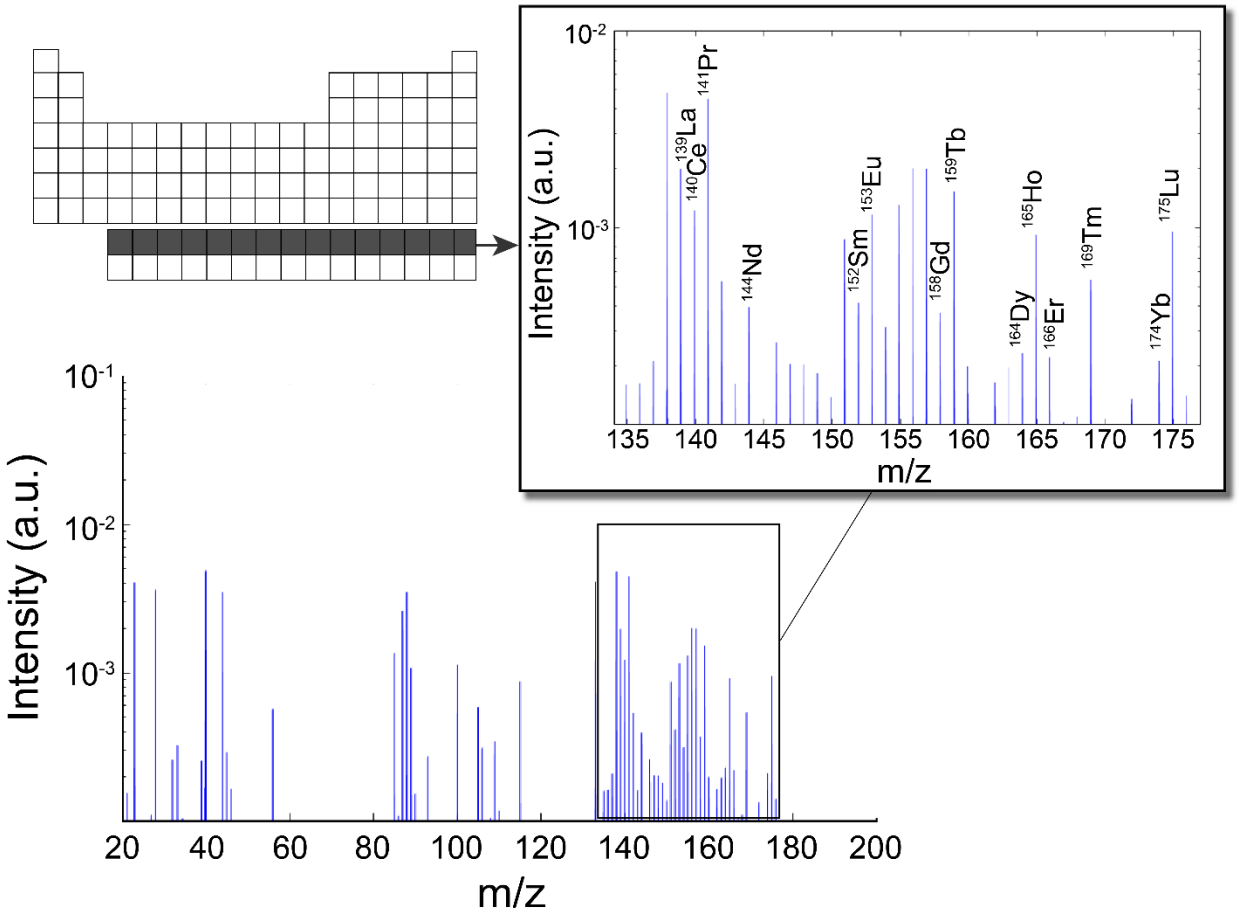

Fig. 5. The Orbitrap LDMS instrument can detect trace elements down to ppmw concentrations, as illustrated by the measurement of REE in NIST SRM610. Observed signal intensities reflect the distinct isotopic compositions and first ionization energies of each element. The detection limit for Pr, which is monoisotopic and has the lowest first ionization energy of the REE, is 1.8 ppmw based on the observed signal-to-noise ratio in this single spectrum. Summing multiple scans can reduce the noise floor and improve detection limits when time and energy resources are available. Irradiance 0.6 GW/cm^2.

Methods

Sample preparation. A 2.2 mm thick CsI finely ground disc (7.49 mm diameter) produced by Almaz Optics, Inc. was secured via interference fit inside a counter bore machined into the stainless sample plate and analyzed daily to tune the voltages applied to the ion optical lenses (see Supplement), verify ion transmission and baseline performance, and monitor for instrumental drift. In order to simulate a salt-rich ice sample from a potentially viable ocean world, a volume of deionized water (Milli-Q, 18.2 MΩ·cm resistivity at room temperature) was physically admixed with 0.32 wt.% KCl (Sigma-Aldrich P9541; purity ≥ 99.0%), approaching the observed alkali salt content of Type III Enceladus plume ice particles collected by the Cassini CDA [36] and modeled salinity levels in Europa's ocean based on brine mobility in the ice crust [51]. The salt solution was doped with 190 ppmw thymine (Alfa Aesar A15879; 97%) and 280 ppmw L-histidine (Sigma Aldrich P500108; 99.9%), both prospective biomarkers (see Supplement). The organic-bearing sample was then agitated with a vortex mixer (2800 rpm) to promote dissolution and homogenization. Prior to drop-casting, the sample plate was cleaned with isopropyl alcohol and acetone in sequence. 40 μL of the analog solution were deposited onto the surface of the stainless steel sample plate over an area of 350 mm^2 and allowed to evaporate on a hot plate (115 °C) in a chemical fume hood; this desiccation step produced a heterogenous residue in line with what might be expected if an aliquot of ice was sublimated on a warm sample plate on a landed mission to Europa or Enceladus. The resultant sample residuum had an average area density of 180 pmol/mm^2 thymine and 210 pmol/mm^2 histidine.

Measurement protocol. The Orbitrap analyzer was located inside a Kimball Physics spherical cube vacuum chamber at pressure conditions found on the surface of Europa (*i.e.*, ≤ 10^{-6} Pa). A load lock chamber equipped with a dedicated pumping system and manual gate valve enabled isolation of the stainless steel plate during sample exchange, minimizing communication between the simulation chamber and laboratory atmosphere. After the sample was loaded onto the target plate, it was introduced to the Orbitrap chamber through the load lock via a linear-rotary actuator. The pressures in both chambers were monitored via hot-cathode ionization vacuum gauges; all analyses were conducted at pressures ≤ 4×10^{-6} Pa. Light emitted from the laser source (266 nm) passed through a fused silica viewport window (>90% transmission at 266 nm) installed on the main vacuum chamber and irradiated the sample at an incident angle of 45°. The laser beam profile at the sample surface was measured at 80 × 120 μm, enabling fluences between 0.06 J/cm^2 (at 1% max energy output) and 6 J/cm^2 (at 100% max energy output), and irradiances between 0.01 GW/cm^2 and 1 GW/cm^2. An external photodiode served to both detect each laser pulse and trigger subsequent operations (*e.g.*, voltage slewing) via a precise timing engine implemented in an FPGA. Different sampling locations on the target plate were accessed by rotating the actuator.

Data processing. Each spectrum was collected at a sampling rate of 5 MHz for either 200 ms (medium-resolution) or 800 ms (high-resolution) transients. A custom LabVIEW based software package [52] was used to regulate experimental sequences, including timing operations, voltage settings and ramp rates, data acquisition, and data processing. Standard data processing techniques included applying Hanning apodization and zero filling raw transient spectra prior to converting the signals to the frequency domain signal via FFT (see Supplement). Each frequency spectrum was calibrated and translated into a conventional mass spectrum using a single peak

(*e.g.*, $^{133}Cs^{+}$) as an internal standard, and two or more well-characterized peaks (*e.g.*, $^{133}Cs^{+}$ and $^{208}Pb^{+}$) to apply an additional linear term to the calibration. Mass accuracy was calculated as the deviation of the determined mass from the exact mass in parts per million. Mass resolving powers, calculated at Full Width at Half Maximum (FWHM) peak intensities, were determined using Gaussian peak fitting functions. To determine CCS, a peak of interest was isolated in the frequency domain and moved artificially to a lower frequency (reducing computing requirements); an inverse FFT enabled reconstruction of the decay profile of the selected ion packet. Chemical species with low signal to noise ratios (*e.g.*, S/N < 10) were excluded from this practice because the high noise floor distorted peak shapes, resulting in inaccurate inversions of the decay profiles.

Acknowledgements

This study was supported by NASA ROSES ICEE 2 Grant 80NSSC19K0610 (PI: Arevalo Jr.) and DALI Grant 80NSSC19K0768 (PI: Arevalo Jr.).

Author contributions are as follows:

NAME	WRITING	EDITING	DATA COLLECTION	DATA ANALYSIS	INSTRUMENT DESIGN	CONCEPT OF OPERATIONS
Ricardo Arevalo Jr.	X		X	X	X	X
Lori Willhite	X	X	X	X		
Anais Bardyn	X	X	X	X		
Ziqin Ni	X	X		X		
Soumya Ray		X	X	X		
Adrian Southard		X	X		X	X
Ryan Danell		X			X	X
Andrej Grubisic		X			X	X
Cynthia Gundersen		X			X	
Niko Minasola		X			X	
Anthony Yu		X			X	
Molly Fahey		X			X	
Emanuel Hernandez		X			X	
Christelle Briois		X			X	
Laurent Thirkell					X	
Fabrice Colin					X	
Alexander Makarov					X	

References

1. Johnson, S.S., et al., *Fingerprinting Non-Terran Biosignatures.* Astrobiology, 2018. **18**(7): p. 915-922.
2. Marshall, S.M., A.R.G. Murray, and L. Cronin, *A probabilistic framework for identifying biosignatures using Pathway Complexity.* Philosophical Transactions of the Royal Society A: Mathematical, Physical and Engineering Sciences, 2017. **375**(2109): p. 20160342.
3. Chan, M.A., et al., *Deciphering Biosignatures in Planetary Contexts.* Astrobiology, 2019. **19**(9): p. 1075-1102.
4. Neveu, M., et al., *The Ladder of Life Detection.* Astrobiology, 2018. **18**(11): p. 1375-1402.
5. Lukmanov, R.A., et al., *On Topological Analysis of fs-LIMS Data. Implications for in Situ Planetary Mass Spectrometry.* Frontiers in Artificial Intelligence, 2021. **4**.
6. Johnston, S., et al., *Small-volume U–Pb zircon geochronology by laser ablation-multicollector-ICP-MS.* Chemical Geology, 2009. **259**(3): p. 218-229.
7. Sagdeev, R.Z. and A.V. Zakharov, *Brief history of the Phobos mission.* Nature, 1989. **341**(6243): p. 581-585.
8. Managadze, G.G., et al., *Study of the main geochemical characteristics of Phobos' regolith using laser time-of-flight mass spectrometry.* Solar System Research, 2010. **44**(5): p. 376-384.
9. Goesmann, F., et al., *The Mars Organic Molecule Analyzer (MOMA) Instrument: Characterization of Organic Material in Martian Sediments.* Astrobiology, 2017. **17**(6-7): p. 655-685.
10. Grubisic, A., et al., *Laser Desorption Mass Spectrometry at Saturn's moon Titan.* International Journal of Mass Spectrometry, 2021. **470**: p. 116707.
11. Chumikov, A.E., et al., *LASMA-LR Laser-Ionization Mass Spectrometer Onboard Luna-25 and Luna-27 Missions.* Solar System Research, 2021. **55**(6): p. 550-561.
12. Briois, C., et al., *Orbitrap mass analyser for in situ characterisation of planetary environments: Performance evaluation of a laboratory prototype.* Planetary and Space Science, 2016. **131**: p. 33-45.
13. Willhite, L., et al., *CORALS: A Laser Desorption/Ablation Orbitrap Mass Spectrometer for In Situ Exploration of Europa.* IEEE Aerospace, 2021.
14. Makarov, A.A., *Mass spectrometer (Patent 5,886,346)*. 1999, HD Technologies Limited, Manchester, United Kingdom. p. 10.
15. Arevalo Jr, R., Z. Ni, and R.M. Danell, *Mass spectrometry and planetary exploration: A brief review and future projection.* Journal of Mass Spectrometry, 2020. **55**(1): p. e4454.
16. Makarov, A., *Electrostatic Axially Harmonic Orbital Trapping: A High-Performance Technique of Mass Analysis.* Analytical Chemistry, 2000. **72**(6): p. 1156-1162.
17. Arevalo Jr, R., et al., *An Orbitrap-based laser desorption/ablation mass spectrometer designed for spaceflight.* Rapid Communications in Mass Spectrometry, 2018.
18. Yu, A.W., et al. *The Lunar Orbiter Laser Altimeter (LOLA) laser transmitter*. in *2011 IEEE International Geoscience and Remote Sensing Symposium*. 2011.
19. Malloci, G., G. Mulas, and C. Joblin, *Electronic absorption spectra of PAHs up to vacuum UV.* A&A, 2004. **426**(1): p. 105-117.
20. Cloutis, E.A., et al., *Ultraviolet spectral reflectance properties of common planetary minerals.* Icarus, 2008. **197**(1): p. 321-347.
21. Fahey, M., et al., *Ultraviolet Laser Development for Planetary Lander Missions.* IEEE Aerospace (Big Sky, MT), 2020: p. 11 pp.
22. Büttner, A., et al. *Optical design and characterization of the MOMA laser head flight model for the ExoMars 2020 mission*. in *Proc.SPIE*. 2019.

23. Jenner, F.E. and H.S.C. O'Neill, *Major and trace analysis of basaltic glasses by laser-ablation ICP-MS.* Geochemistry, Geophysics, Geosystems, 2012. **13**(3).
24. Humayun, M., F.A. Davis, and M.M. Hirschmann, *Major element analysis of natural silicates by laser ablation ICP-MS.* Journal of Analytical Atomic Spectrometry, 2010. **25**(7): p. 998-1005.
25. Longerich, H.P., D. Günther, and S.E. Jackson, *Elemental fractionation in laser ablation inductively coupled plasma mass spectrometry.* Fresenius' Journal of Analytical Chemistry, 1996. **355**(5): p. 538-542.
26. Alterman, M.A., N.V. Gogichayeva, and B.A. Kornilayev, *Matrix-assisted laser desorption/ionization time-of-flight mass spectrometry-based amino acid analysis.* Analytical Biochemistry, 2004. **335**(2): p. 184-191.
27. Sarracino, D. and C. Richert, *Quantitative MALDI-TOF MS of oligonucleotides and a nuclease assay.* Bioorganic & Medicinal Chemistry Letters, 1996. **6**(21): p. 2543-2548.
28. Chumbley, C.W., et al., *Absolute Quantitative MALDI Imaging Mass Spectrometry: A Case of Rifampicin in Liver Tissues.* Analytical Chemistry, 2016. **88**(4): p. 2392-2398.
29. Zubarev, R.A. and A. Makarov, *Orbitrap Mass Spectrometry.* Analytical Chemistry, 2013. **85**(11): p. 5288-5296.
30. Makarov, A., et al., *Dynamic range of mass accuracy in LTQ orbitrap hybrid mass spectrometer.* Journal of the American Society for Mass Spectrometry, 2006. **17**(7): p. 977-982.
31. Hoegg, E.D., et al., *Isotope ratio characteristics and sensitivity for uranium determinations using a liquid sampling-atmospheric pressure glow discharge ion source coupled to an Orbitrap mass analyzer.* Journal of Analytical Atomic Spectrometry, 2016. **31**(12): p. 2355-2362.
32. Hofmann, A.E., et al., *Using Orbitrap mass spectrometry to assess the isotopic compositions of individual compounds in mixtures.* International Journal of Mass Spectrometry, 2020. **457**: p. 116410.
33. Hardouin, J., *Protein sequence information by matrix-assisted laser desorption/ionization in-source decay mass spectrometry.* Mass Spectrometry Reviews, 2007. **26**(5): p. 672-682.
34. Franchi, M., J.P. Ferris, and E. Gallori, *Cations as Mediators of the Adsorption of Nucleic Acids on Clay Surfaces in Prebiotic Environments.* Origins of life and evolution of the biosphere, 2003. **33**(1): p. 1-16.
35. Trumbo, S.K., M.E. Brown, and K.P. Hand, *Sodium chloride on the surface of Europa.* Science Advances, 2019. **5**(6): p. eaaw7123.
36. Postberg, F., et al., *A salt-water reservoir as the source of a compositionally stratified plume on Enceladus.* Nature, 2011. **474**: p. 620.
37. De Sanctis, M.C., et al., *Fresh emplacement of hydrated sodium chloride on Ceres from ascending salty fluids.* Nature Astronomy, 2020. **4**(8): p. 786-793.
38. Hand, K.P., et al., *Report of the Europa Lander Science Definition Team*. 2017, NASA HQ: Washington, DC.
39. Hendrix, A.R., et al., *The NASA Roadmap to Ocean Worlds.* Astrobiology, 2018. **19**(1): p. 1-27.
40. Waite Jr, J.H., et al., *Liquid water on Enceladus from observations of ammonia and 40Ar in the plume.* Nature, 2009. **460**(7254): p. 487-490.
41. Altwegg, K., H. Balsiger, and S.A. Fuselier, *Cometary Chemistry and the Origin of Icy Solar System Bodies: The View After Rosetta.* Annual Review of Astronomy and Astrophysics, 2019. **57**(1): p. 113-155.
42. Guzman, M., et al., *Collecting amino acids in the Enceladus plume.* International Journal of Astrobiology, 2018. **18**(1): p. 47-59.
43. Takayama, M., *In-source decay characteristics of peptides in matrix-assisted laser desorption/ionization time-of-flight mass spectrometry.* Journal of the American Society for Mass Spectrometry, 2001. **12**(4): p. 420-427.

439 44. Katta, V., D.T. Chow, and M.F. Rohde, *Applications of In-Source Fragmentation of Protein Ions for*
440 *Direct Sequence Analysis by Delayed Extraction MALDI-TOF Mass Spectrometry.* Analytical
441 Chemistry, 1998. **70**(20): p. 4410-4416.
442 45. Sanders, J.D., et al., *Determination of Collision Cross-Sections of Protein Ions in an Orbitrap Mass*
443 *Analyzer.* Analytical Chemistry, 2018. **90**(9): p. 5896-5902.
444 46. Makarov, A. and E. Denisov, *Dynamics of ions of intact proteins in the Orbitrap mass analyzer.*
445 Journal of the American Society for Mass Spectrometry, 2009. **20**(8): p. 1486-1495.
446 47. Anupriya, C.A. Jones, and D.V. Dearden, *Collision Cross Sections for 20 Protonated Amino Acids:*
447 *Fourier Transform Ion Cyclotron Resonance and Ion Mobility Results.* Journal of the American
448 Society for Mass Spectrometry, 2016. **27**(8): p. 1366-1375.
449 48. Chyba, C. and C. Sagan, *Endogenous production, exogenous delivery and impact-shock synthesis*
450 *of organic molecules: an inventory for the origins of life.* Nature, 1992. **355**(6356): p. 125-132.
451 49. Poppe, A.R., *An improved model for interplanetary dust fluxes in the outer Solar System.* Icarus,
452 2016. **264**: p. 369-386.
453 50. Taylor, S.R. and S.M. McLennan, *The significance of the rare earths in geochemistry and*
454 *cosmochemistry*, in *Handbook on the Physics and Chemistry of Rare Earths*. 1988, Elsevier. p.
455 485-578.
456 51. Steinbrügge, G., et al., *Brine Migration and Impact-Induced Cryovolcanism on Europa.*
457 Geophysical Research Letters, 2020. **47**(21): p. e2020GL090797.
458 52. Danell, R., et al., *A Full Featured, Flexible, and Inexpensive 2D and 3D Ion Trap Control*
459 *Architecture and Software Package.* Proceedings of the 58th ASMS Conference on Mass
460 Spectrometry and Allied Topics (Salt Lake City, UT), 2010.

461